The ERM proteins interact with the HOPS complex to regulate the maturation of endosomes

Dafne Chirivino[a], Laurence Del Maestro[a], Etienne Formstecher[b], Philippe Hupé[c], Graça Raposo[d], Daniel Louvard[a], and Monique Arpin[a]

[a]Institut Curie-Unité Mixte de Recherche 144 (UMR144), Centre National de la Recherche Scientifique (CNRS)/ Morphogenèse et Signalisation cellulaires, 75248 Paris Cedex 05, France; [b]Hybrigenics, Paris 75014, France; [c]Institut Curie-UMR144, CNRS/INSERM U900/Ecole des Mines, Fontainebleau 77300, France; [d]Institut Curie-UMR144 CNRS/Structure et compartimentation membranaire, 75248 Paris Cedex 05, France

ABSTRACT In the degradative pathway, the progression of cargos through endosomal compartments involves a series of fusion and maturation events. The HOPS (homotypic fusion and protein sorting) complex is part of the machinery that promotes the progression from early to late endosomes and lysosomes by regulating the exchange of small GTPases. We report that an interaction between subunits of the HOPS complex and the ERM (ezrin, radixin, moesin) proteins is required for the delivery of EGF receptor (EGFR) to lysosomes. Inhibiting either ERM proteins or the HOPS complex leads to the accumulation of the EGFR into early endosomes, delaying its degradation. This impairment in EGFR trafficking observed in cells depleted of ERM proteins is due to a delay in the recruitment of Rab7 on endosomes. As a consequence, the maturation of endosomes is perturbed as reflected by an accumulation of hybrid compartments positive for both early and late endosomal markers. Thus, ERM proteins represent novel regulators of the HOPS complex in the early to late endosomal maturation.

INTRODUCTION

ERM (ezrin, radixin, moesin) proteins are membrane–cytoskeleton linkers involved in the assembly of specialized domains of the membrane. Their association with both the membrane proteins and actin filaments is regulated and requires conformational activation (Bretscher et al., 2002). ERM proteins consist of a globular head domain known as the FERM (four-point one, ezrin, radixin, moesin) domain that binds numerous membrane and membrane-associated proteins. This domain is followed by a region rich in α-helices. The last 30 C-terminal amino acids contain the F-actin binding site (Turunen et al., 1994). ERM proteins exist in a closed conformation due to a strong interaction between the amino-terminal domain and the ~100 C-terminal amino acids (N- and C-ERM association domain; ERMAD) in which the membrane and actin binding sites are masked (Gary and Bretscher, 1995). The intramolecular interaction is relieved by the sequential binding of the FERM domain to phosphatidylinositol 4,5-bi-phosphate (PIP2) and the phosphorylation of a conserved threonine residue in the F-actin binding site (Fiévet et al., 2004). The "open" state therefore can interact with its binding partners and is mainly detected at the plasma membrane. The major pool of ERM proteins in the cell, however, is present in the cytoplasm where it is thought to be in an inactive conformation.

Through their dynamic and reversible interactions with the membrane proteins and actin filaments, ERM proteins coordinate signal transduction with cytoskeleton remodeling and membrane protein transport and activity. ERM proteins were shown to regulate the trafficking and the activity of several transporters and receptors. In particular, ERM proteins have been involved in trafficking events from or to the plasma membrane. Indeed, the recycling of transmembrane proteins such as the α1β-adrenergic receptor (Stanasila et al., 2006), NHE3 (Zhao et al., 2004; Cha

et al., 2006), H-K-ATPase (Zhou et al., 2005), and transferrin receptor (Barroso-Gonzalez et al., 2009) requires the ERM proteins.

The precise role of ERM proteins in membrane protein trafficking is not understood at the mechanistic level. Neither is it known at which step of endocytosis/exocytosis they are involved and how they interact with the transport machinery. It has been proposed that ERM proteins function at the interface with the plasma membrane regulating trafficking of vesicles (Zhou et al., 2003; Tamma et al., 2005; Cha et al., 2006). Several studies, however, localized ERM proteins on internal compartments in addition to their presence at the plasma membrane. ERM proteins have been localized on early/recycling endosomes (Harder et al., 1997; Stanasila et al., 2006; Morel et al., 2009) and clathrin-coated vesicles (Barroso-Gonzalez et al., 2009). Interestingly, they also have been observed being associated with compartments of the degradative pathway, such as lysosomes (Poupon et al., 2003) and phagosomes (Defacque et al., 2000).

Here we describe an interaction between ERM proteins and one subunit of the HOPS (hemolytic fusion and protein sorting) complex, Vps11. Vps11 is one of the four subunits of the core C Vps complex, which associates with two accessory subunits Vps39 and Vps41 to form the HOPS complex. Recently a CORVET complex has been characterized in yeast that shares with the HOPS complex the same C-Vps core proteins, including Vps11, but possesses alternative accessory subunits to the Vps41/Vps39 proteins, the subunits Vps3 and Vps8 (Peplowska et al., 2007). These two complexes stimulate Rab GTPase nucleotide exchange, the HOPS complex interacting with Ypt7p, the *Saccharomyces cerevisiae* Rab7 orthologue (Wurmser et al., 2000), and the CORVET complex with the Rab5 homologue, Vps21 (Peplowska et al., 2007). Whereas the HOPS complex is highly conserved from yeast to mammals (Rieder and Emr, 1997; Seals et al., 2000; Huizing et al., 2001), the CORVET complex has not yet been identified in mammalian cells but likely exists given the high similarity in the transport machinery between yeast and mammals. In yeast, the class C Vps/HOPS complex was characterized as a tethering complex required for homotypic fusion at the vacuole (Wurmser et al., 2000). In higher eukaryotes, this complex is involved in the delivery of endocytosed macromolecules to late endosomes and lysosomes or lysosome-related pathways (Sevrioukov et al., 1999; Suzuki et al., 2003; Pulipparacharuvil et al., 2005; Maldonado et al., 2006). The transport of cargos to lysosomes and lysosome-related organelles involves the conversion of the early Rab5- into late Rab7-positive endosomes. The HOPS complex has been shown to play a role in this process by acting as an effector of Rab5 and an activator of Rab7 (Rink et al., 2005). Although the subunit Vps39p has been proposed to have a nucleotide exchange activity toward Ypt7p (Wurmser et al., 2000; Rink et al., 2005), recent work suggests that this exchange activity is carried by the complex Mon-Ccz1, an interactor of the HOPS complex (Nordmann et al., 2010).

Given the role of the HOPS complex in the degradative pathway, we addressed the function of ezrin/Vps11 interaction in the internalization of the EGF receptor (EGFR). We report that the ERM proteins are required for the delivery of the EGFR to lysosomes. We propose that ERM proteins modulate the kinetic of recruitment of Rab7 by the HOPS complex, therefore tuning the maturation of endosomes.

RESULTS
The ERM proteins interact with Vps11, a subunit of the HOPS complex
In yeast two-hybrid screens performed with ezrin constructs as baits we identified a new ezrin partner, Vps11, a subunit of the HOPS complex. Several independent clones that cover a domain pre-

dicted to form a coiled-coil structure (amino acids [aa] 643–819) were found in two independent screens performed with either the C-terminal domain of ezrin (aa 309–586) or ezrin deleted of the last 52 aa (1–535). No interaction was found with the amino-terminal domain of ezrin (aa 1–310). Because the minimal domain on ezrin that binds Vps11 corresponds to the region (aa 309–535) that contains α-helical structures, it suggests that the two proteins interact through their coiled-coil regions (Figure 1A). The interaction between the full-length Vps11 and ezrin was confirmed by immunoprecipitation and GST-pull down (Figure 1, B and C). No binding of Vps11 to the C-terminal domain of ezrin was detected, however, in GST pull down unlike what was observed in the two-hybrid screen (Figure 1C). A possible explanation is that the α-helical domain of ezrin fused to GST has an altered conformation, therefore preventing its association with Vps11. Alternatively, a factor able to interact with the C-terminal domain of ezrin alone may interfere with the binding of Vps11. Given the high degree of conservation among ERM proteins, we determined whether radixin and moesin would also interact with Vps11. Interestingly, Vps11 was found to interact with radixin and moesin as well (Figure 1D).

Ezrin and Vps11 localize on endosomal structures
To characterize the cellular localization of Vps11, we established HeLa cell lines stably expressing myc-Vps11 at a level similar to that of the endogenous protein (unpublished data). In these cells, Vps11 was present in punctuated structures that partially colocalize with early and late endosomal markers, the Rab5 effector EEA1 (early endosome antigen 1) (Simonsen et al., 1998), and LAMP-1 (lysosomal-associated membrane protein 1), respectively (Figure 2A). The endosomal distribution of Vps11 prompted us to verify whether a pool of ezrin, in addition to its well-described localization at the plasma membrane, was present on endosomes. We confirmed, by immunoelectron microscopy, that ezrin is not exclusively localized at the cell surface, but it is also associated with intracellular tubulovesicular compartments with morphological features of endosomes (Figure 2B). These data suggest that ezrin and Vps11 might cooperate at the level of the endosomes.

Depletion of either Vps11 or ERM proteins delays EGF transport through EEA1-positive compartments
Given the role of the HOPS complex in the degradative pathway, we addressed the function of ezrin/Vps11 interaction in the internalization of EGFR. To follow the delivery of EGFR to lysosomes, myc-Vps11 HeLa cells were stimulated with EGF in presence of cycloheximide, and the receptor level was analyzed at different time points in control cells and in cells depleted of either ezrin or Vps11. Using two independent sets of small interfering RNA (siRNA), we observed a striking delay in EGFR degradation in cells depleted of Vps11 compared to mock cells (Figure 3; see Supplemental Figure S1 for the second set of siRNA). No detectable effect of ezrin depletion was observed on EGFR degradation (unpublished data), suggesting that a compensatory effect by radixin and/or moesin may operate in these cells. We therefore inactivated the three ERM proteins and we observed a delay in the kinetics of EGFR degradation too (Figure 3; also see Figure S1 for the second set of siRNA).

Next we sought to determine at which step of EGFR transport the HOPS complex and ERM proteins were involved. Internalization of fluorescently labeled EGF for 15 min followed by a chase for various time points were performed in myc-Vps11 HeLa cells depleted of either Vps11 or ERM proteins. EGF transit through EEA1 compartments was analyzed by wide-field three-dimensional (3D) sectioning microscopy followed by quantitative single cell analysis. We determined the fraction of total EGF area that overlapped with
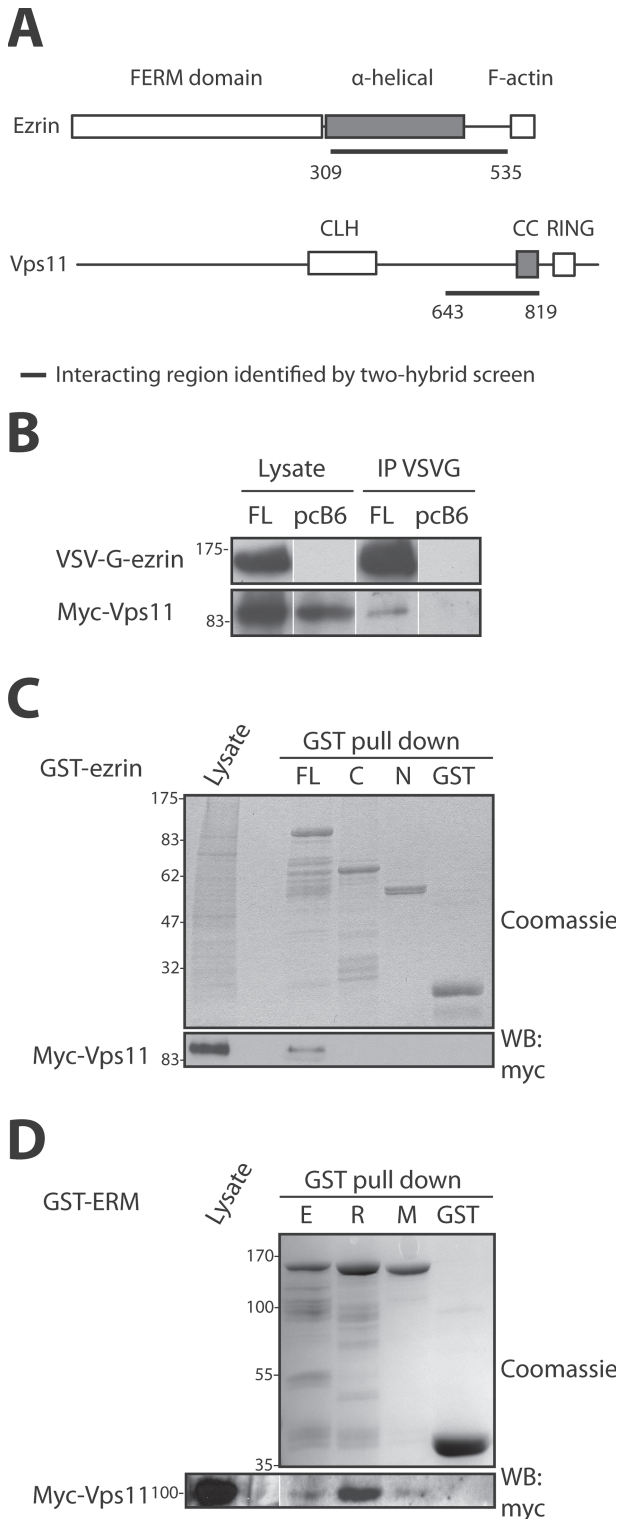
A

FERM domain   α-helical   F-actin

Ezrin

309   535

CLH   CC RING

Vps11

643   819

— Interacting region identified by two-hybrid screen

B

Lysate | IP VSVG
FL pcB6 | FL pcB6

VSV-G-ezrin 175-

Myc-Vps11 83-

C

GST-ezrin

Lysate | GST pull down
FL C N GST

175-
83-
62-
47-
32-

Coomassie

Myc-Vps11 83-

WB: myc

D

GST-ERM

Lysate | GST pull down
E R M GST

170-
100-
55-
35-

Coomassie

Myc-Vps11 100-

WB: myc

FIGURE 1: Interaction of ERM proteins with Vps11. (A) Modular organization of ezrin and Vps11. Ezrin contains a globular N-terminal domain (FERM domain) followed by a region rich in α-helices and an F-actin binding site located within the last C-terminal amino acids (Bretscher *et al.*, 2002). Vps11 contains a clathrin heavy chain repeat (CLH) followed by a coiled-coil region (CC) and a RING-finger domain (RING) (Nickerson *et al.*, 2009). The minimal interacting regions identified in yeast two-hybrid screens are underlined. (B) The cDNA coding for myc-Vps11 was cotransfected with the cDNA coding for VSV-G–tagged ezrin (FL) or the empty vector pcB6 (pcB6). Immunoprecipitation of ezrin was performed with the anti-VSVG

antibody, and Vps11 was detected with an anti-myc antibody. (C) Immobilized GST or GST fused to ezrin FL, ezrin C-terminal (C), or ezrin N-terminal (N) were incubated with lysates from cells expressing myc-Vps11. Vps11 interacts only with full-length ezrin. (D) Immobilized GST and GST fused to ezrin (E), radixin (R), or moesin (M) were incubated with a lysate from cells expressing myc-Vps11. Vps11 interacts with the three ERM proteins.

EEA1 in ~50 cells for each time point. Only cells in which proteins were efficiently depleted were included in the analysis. Immediately after the pulse (0-min chase) we observed, in cells depleted of Vps11 or ERM proteins, a smaller level of colocalization between EGF and EEA1 compared to control cells transfected with scramble siRNA (Figure 4A and Supplemental Figure S2A). This observation indicated that, in the absence of Vps11 or ERM proteins, the transport of EGF toward the early endosomes is delayed. During the remaining chasing time, we observed that the colocalization between EGF and EEA1 decreased in control cells, indicating that EGF has exited from early endosomes (Figures 4B and S2B). In contrast, in cells depleted of Vps11 or ERM proteins, an increased colocalization between EGF and EEA1 positive compartments at 15-min chase was observed. Given the delay of EGF to enter into the early compartments in silenced cells, the observed accumulation of EGF into EEA1 compartments indicated that the exit of EGF from these compartments was also affected. This delay was maintained at later time points because after 60-min chase the colocalization between EGF and EEA1 in cells depleted of Vps11 or ERM proteins was still higher when compared to that observed in control cells. Interestingly, the depletion of Vps11 led to aggregated EEA1-positive compartments that were not observed in cells depleted of ERM proteins (Figure 4B and Figure S2B insets), indicating that Vps11 is dispensable for the tethering of early endosomes but is required for their homotypic fusion. Altogether, these data showed that both the HOPS complex and ERM proteins are required for EGF transit through EEA1 compartments.

ERM proteins and the HOPS complex regulate the transport of EGFR from early to late endosomes

Because Vps11 or ERM protein depletion caused a delay in the exit of EGF from early endosomes, we then asked whether the delivery of EGFR to late endosomes was also affected. We determined the amount of EGF colocalizing with Rab7 after 60 min of chase in myc-Vps11 HeLa cells transiently expressing GFP-Rab7. The quantification was performed on single cells (as described earlier in this article) that expressed low levels of GFP-Rab7 to exclude any effects of overexpression. The level of colocalization between EGF and Rab7 was calculated as a percentage of the total EGF present in the cells at 60 min. In cells depleted of either Vps11 or ERM proteins, we observed a decrease in the colocalization between EGF and Rab7 compared to cells treated with scrambled siRNA (Figure 5, A and B and Figure S3). These data indicated that both ERM proteins and the HOPS complex positively regulate the transport of EGFR to the late endosomes. Therefore, we tested whether the overexpression of ERM proteins could accelerate the delivery of EGF to Rab7 compartments. Indeed, ezrin overexpression significantly increased the level of colocalization between EGF- and Rab7-positive compartments at 60-min chase (Figure 6A). These data confirmed that ERM proteins facilitate the delivery of EGFR to the Rab7 compartments. To determine if this increased colocalization with Rab7 required the HOPS complex, we overexpressed ezrin in myc-Vps11 HeLa cells depleted or not of Vps11. Cells overexpressing ezrin and treated with scrambled siRNA showed an increased colocalization of EGF
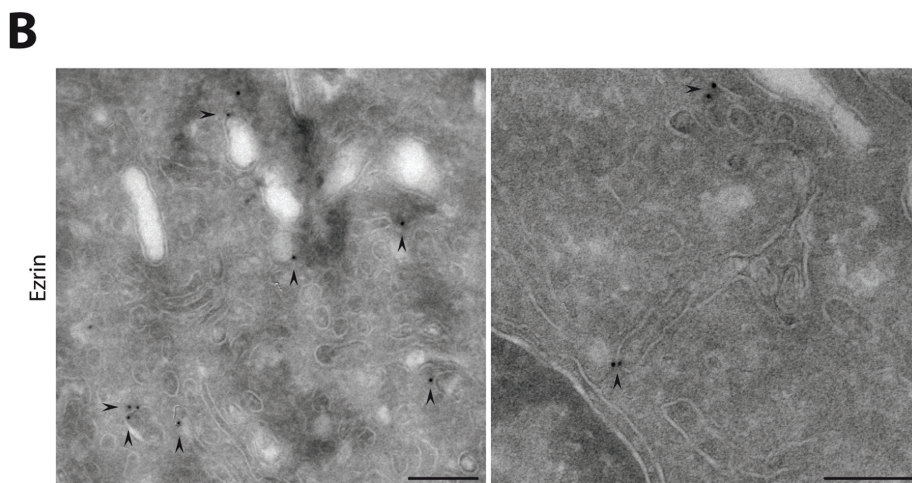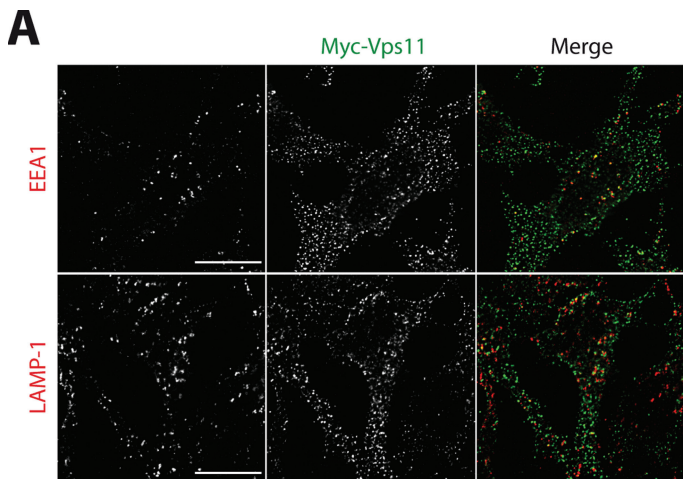
FIGURE 2: Ezrin and Vps11 localize to endosomal compartments. (A) Localization of Vps11 in myc-Vps11 HeLa cells. Double immunofluorescence was performed with anti-myc antibody (green) and either anti-EEA1 or anti-LAMP1 antibodies (red). Images were taken with a 3D wide-field optical sectioning microscope. Each image corresponds to a maximum-intensity Z projection performed after deconvolution. The merged images indicate a partial colocalization of Vps11 with either EEA1 or LAMP1. Scale bar: 10 μm. (B) The two panels show immunogold labeling on ultrathin cryosections of myc-Vps11 HeLa cells treated with EGF (50 ng/ml) for 15 min. Sections were labeled using an anti-ezrin antibody and protein A gold (PAG10). Labeling is observed in tubulovesicular membranes. Scale bar: 200 nm.
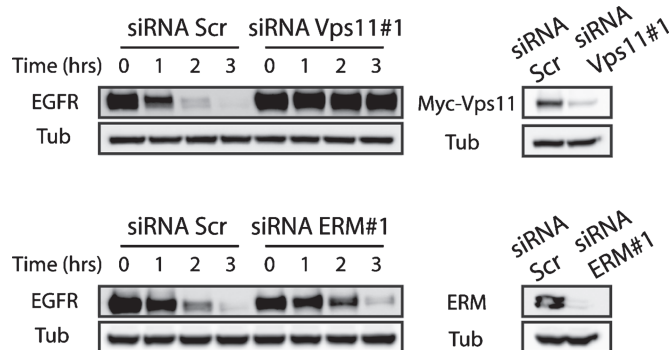

FIGURE 3: Time course of EGFR degradation in myc-Vps11 HeLa cells treated with scramble siRNA (Scr) or siRNA targeting either Vps11 (top panel) or ERM proteins (bottom panel). Tubulin (Tub) serves as a loading control. Right panels show the extent of depletion after siRNA treatment. The blots shown are representative of multiple independent experiments.

with Rab7 compared to mock cells transfected with an empty vector. In cells depleted of Vps11, no increase in the colocalization of EGF with Rab7 was observed, indicating that the effect of ezrin on the transport of EGFR to Rab7-positive endosomes is dependent on the HOPS complex (Figure 6B).

ERM proteins and the HOPS complex are required for the transition from early to late endosomes

Because ezrin overexpression increases the amount of EGFR delivered to the late Rab7-positive endosomes, we determined whether the kinetics of EGFR degradation was accelerated. Surprisingly, we observed a delay in EGFR degradation similar to that observed in the absence of ERM proteins (Figure 6C). In cells overexpressing ezrin, quantitative single cell analysis of the colocalization of EGF with EEA1 revealed a delay of EGF entrance into EEA1-positive compartments (Figure 6D, left) followed by a slight but significant accumulation of EGF in these endosomes (Figure 6D, right). Therefore, overexpression of ezrin led to an increase in EGF localization with both EEA1- and Rab7-positive compartments. These data suggested a defect in the maturation of endosomes, a process in which the HOPS complex has been shown to be involved (Rink *et al.*, 2005; Poteryaev *et al.*, 2010). We therefore asked whether ERM proteins might impair the maturation of endosomes by evaluating the colocalization of GFP-Rab7 with EEA1-positive compartments when cells were stimulated with EGF followed by 60 min of chase. A basal level of colocalization between Rab7 and EEA1 that was observed in cells transfected with the vector alone likely reflects the physiological state of maturation of EEA1/early into Rab7/late endosomes. Strikingly, increased colocalization of Rab7 with EEA1 was observed with both ezrin overexpression and depletion of ERM proteins as compared to control cells, indicating a higher number of Rab7/EEA1 hybrid compartments (Figure 7, A and B). These data indicated that an excess or a lack of ERM proteins lead to the accumulation of EGFR in endosomes that are unable to complete their maturation into late endosomes. In contrast, depletion of Vps11 resulted in a decreased colocalization between Rab7 and EEA1 (Figure 7C). Therefore knockdown of Vps11 leads to defective EEA1 compartments that are unable to undergo both homotypic fusion and maturation, thus drastically reducing the number of hybrid EEA1/Rab7 endosomes.

ERM proteins facilitate Rab7 recruitment on individual endosomes

Our results indicated a regulatory role for ERM proteins in the maturation of early to late endosomes, a process that is dependent on the dynamic of Rab7 recruitment on endosomes by the HOPS complex (Rink *et al.*, 2005; Vonderheit and Helenius, 2005). Because
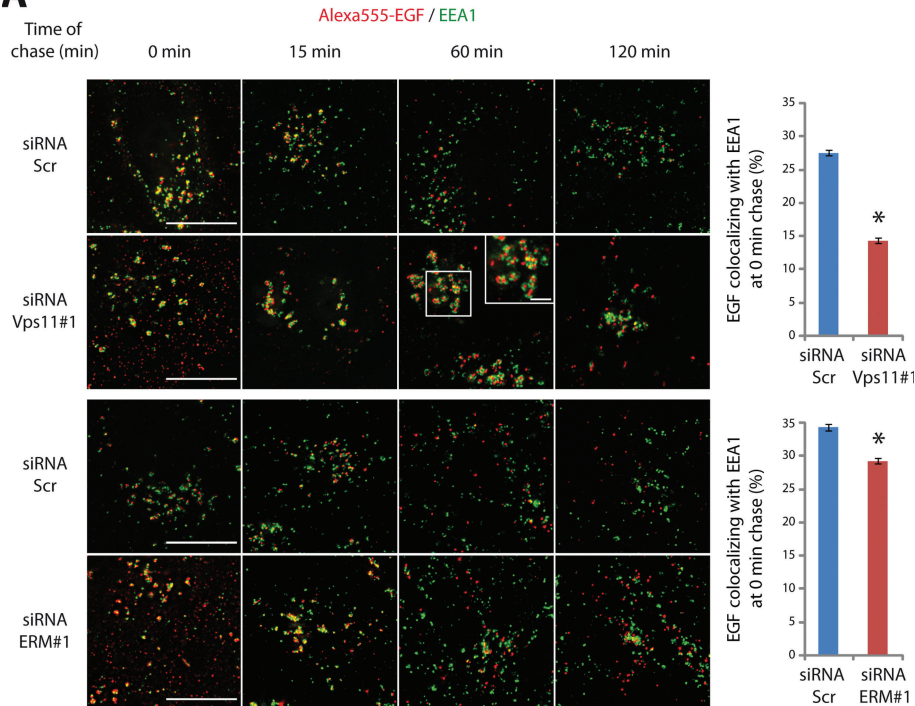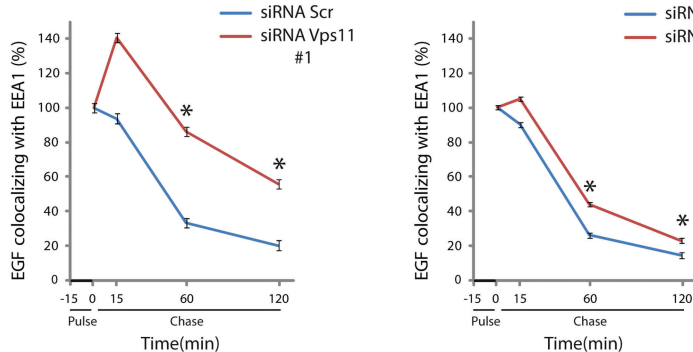
FIGURE 4: EGFR transit through early endosomes is perturbed in cells depleted of either Vps11 or ERM proteins. HeLa myc-Vps11 cells treated with indicated siRNAs were incubated with Alexa555-EGF (red) for 15 min and then chased for the indicated time points. Immunofluorescence was performed with an anti-EEA1 antibody (green). Images were taken with a 3D wide-field optical sectioning microscope. Each image corresponds to a maximum-intensity Z projection performed after deconvolution. Only merged images are shown. Scale bar: 10 μm. Insets show aggregated EEA1 compartments (scale bar: 2 μm). Right panels show the quantification of EGF area that overlaps with EEA1 at 0-min chase expressed as a percentage of total EGF. (B) Quantification of EGF area that overlaps with EEA1 over time expressed as a percentage of the initial EGF colocalization with EEA1 at 0-min chase. Values were statistically tested using a two-way ANOVA. Least-square means ± SEM are plotted (two independent experiments, n ≥ 50 cells for each time point per experiment, * p < 0.001 compared with the control).

somes that were not involved in fusion events were analyzed. In cells transfected with scramble siRNA, the kinetics of Rab7 recruitment was rapid whereas it was considerably reduced in cells depleted of ERM proteins. Because the increase in Rab7 fluorescence fitted a sigmoid distribution, two parameters were analyzed: the slope of the curve and the time required to reach a plateau (see *Materials and Methods*) (Figure 8, A and B; Supplementary Movies 1 and 2). First, we observed that the slope of the curve, α, was smaller in cells depleted of ERM proteins as compared to control cells consistent with a delay in GFP-Rab7 recruitment. Second, we found that the time required for GFP-Rab7 to reach half of the maximum intensity (Δt) was ~16 s in control cells and ~50 s in cells depleted of ERM proteins (Figure 8C). Our data indicate that ERM proteins tune Rab7 recruitment on endosomes.

DISCUSSION

We report here that the ERM proteins interact with Vps11, a subunit of the HOPS complex, and that this interaction is required for the delivery of EGFR to lysosomes. We demonstrate that ERM proteins tune the maturation of endosomes through their interaction with the HOPS complex by modulating the kinetics of recruitment of Rab7 on the endosomes.

We show that Vps11 interacts with full-length ERM proteins through their α-helical domain, suggesting that this binding site is not cryptic. As suggested by the crystal structure of the full-length insect moesin, the α-helical region may be accessible for interaction when ERM proteins are in a closed conformation (Li *et al.*, 2007). The α-helical region covers a large surface area of the FERM domain therefore masking ligand binding sites for PIP2 and membrane proteins (Li *et al.*, 2007). It is therefore possible that the binding of Vps11 to the α-helical domain of ERM proteins induces conformational changes facilitating the opening of the proteins in addition to the well-documented mechanisms involved in the dissociation of the head-to-tail interaction.

We demonstrate that both ERM proteins and the HOPS complex regulate the transport of cargo through the endosomal compartments. Depletion of either ERM proteins or Vps11 led to an accumulation of ERM proteins into early endosomes due to a delay in EGF to both reach the EEA1-positive compartments and to leave them. Similarly, Barroso-Gonzales and colleagues previously reported that depletion of moesin causes an accumulation of the transferrin receptor in Rab5-positive endosomes (Barroso-Gonzales *et al.*, 2009). A defect in cargo exit from Rab5-positive early endosomes has also been observed on depletion of Vps39 in A431 cells (Rink *et al.*, 2005). Whereas Vps39 depletion

the HOPS complex displays a guanine exchange activity toward Rab7, we asked whether ERM proteins could regulate the recruitment and/or activation of Rab7 by enhancing the exchange activity of the HOPS complex toward Rab7. To test this hypothesis, we imaged myc-Vps11 HeLa cells stably expressing moderate levels of GFP-Rab7 during the continuous endocytosis of EGF. We monitored the recruitment of GFP-Rab7 on individual EGF-positive endosomes over time in cells treated with nocodazole to minimize the movement of endosomes. Indeed, nocodazole treatment was previously shown not to affect Rab7 recruitment (Rink *et al.*, 2005). Only endo-
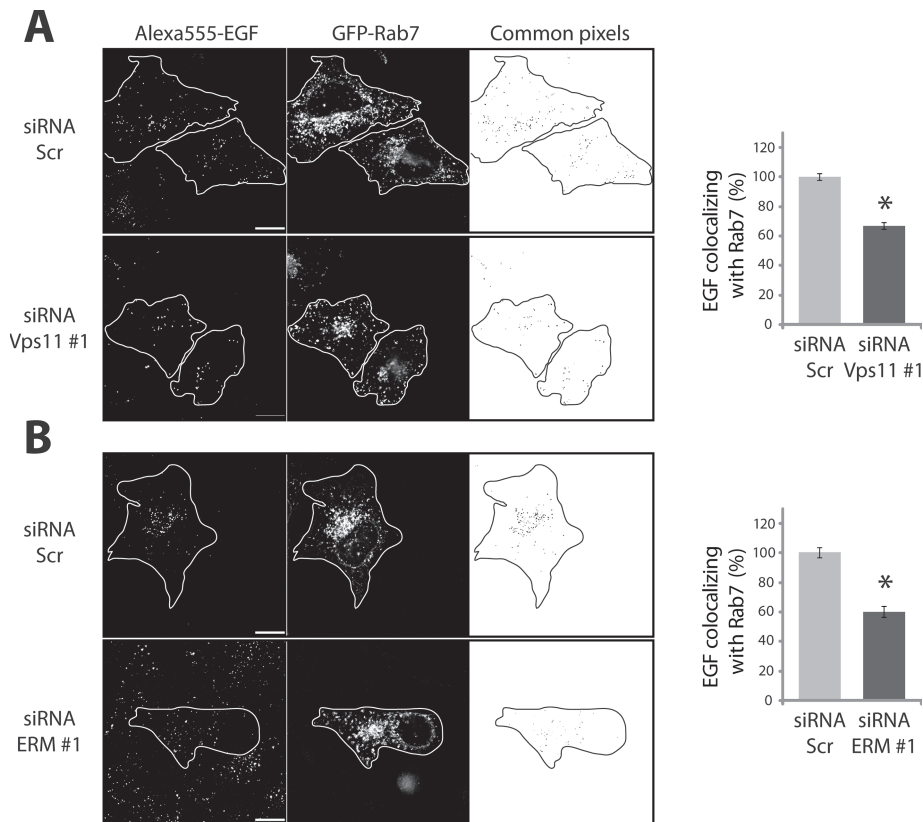
FIGURE 5: ERM proteins and the HOPS complex regulate EGFR transport from early to late endosomes. HeLa myc-Vps11 cells depleted of Vps11 (A) or ERM proteins (B) were transiently transfected with GFP-Rab7 and incubated with Alexa555-EGF (red) for 15 min and then chased for 60 min. Images were taken with a 3D wide-field optical sectioning microscope. On the right are represented the common pixels between the two channels after deconvolution and segmentation. Each image corresponds to a maximum-intensity Z projection. Histograms represent the EGF area that overlaps with Rab7 expressed as a percentage of the colocalization in control cells. Differences in the colocalization between EGF and Rab7 were statistically tested using a two-way ANOVA. Least-square means ± SEM are plotted (two independent experiments, n ≥ 50 cells in each condition per experiment, * p < 0.001). Scale bar: 10 µm.

resulted in an enlargement of EEA1/Rab5-positive early endosomes, we observed that depletion of Vps11 led to aggregated EEA1-positive compartments consistent with a defect in the homotypic fusion of early endosomes. The phenotypic differences observed in early endosomes following Vps11 or Vps39 depletion may be best understood in view of a recent observation that, in yeast, Vps11 is also present in the CORVET complex (Peplowska et al., 2007). In the absence of Vps11, the function of the CORVET complex would be impeded, thus preventing homotypic fusion of early endosomes and resulting in aggregated endosomes. In contrast, depletion of Vps39 does not prevent homotypic fusion because enlarged early endosomes are observed, indicating that Vps39, in the HOPS complex, is involved in a later step of endosome maturation (Rink et al., 2005). Although we could not observe changes in the morphology of early endosomes in cells depleted of ERM proteins, some mild effects might be masked due to the dynamic of the fusion/fission events.

We show that ERM proteins cooperate with the HOPS complex for the transport of EGFR to the late endosomes. Indeed, whereas depletion of ERM proteins delays the transport of EGFR to Rab7-positive compartments, overexpression of ezrin accelerates it, and this effect requires the presence of the HOPS complex. Both ezrin overexpression and depletion of ERM proteins, however, increase the number of hybrid compartments carrying both early and late

endocytic markers, indicating a defect in endosome maturation. This defect correlates with an altered kinetic of Rab7 recruitment mediated by ERM proteins. A similar delay in the recruitment of Rab7 onto endosomes has been reported in A431 cells depleted of Vps39 (Rink et al., 2005). It is worth mentioning that Vps39 was also identified as an ezrin interacting partner in the same yeast two-hybrid screens.

In light of our data, we propose that ERM proteins regulate the maturation of endosomes mediated by the HOPS complex. Transition between early and late endosomes involves an exchange of small GTPases with the recruitment of Rab7 and the dissociation of Rab5. This activity is part of a Rab cascade in which the guanine nucleotide exchange factor (GEF) of a downstream GTPase serves as an effector of an upstream Rab GTPase (Rink et al., 2005; Grosshans et al., 2006). The Rab conversion model predicts that a feedback regulatory loop exists that controls the recruitment of Rab7 and the dissociation of Rab5 by the HOPS complex. Rab7 recruitment on early endosomes would lead, at a certain threshold, to the exchange with Rab5 (Del Conte-Zerial et al., 2008). Our results suggest that ERM proteins may regulate both Rab7 recruitment and Rab5 dissociation. Through their interaction with the HOPS complex, ERM proteins regulate the recruitment of Rab7 on late endosomes. In the absence of ERM proteins, more time is required for Rab7 to reach the threshold that allows the dissociation of Rab5 and its effectors, therefore resulting in the observed increase in EEA1/Rab7-positive compartments. Upon ezrin overexpression, the transport of EGF to Rab7 compartments is accelerated, but the dissociation of the Rab5 effector EEA1 is impaired, resulting in increased EEA1/Rab7-positive compartments. As ERM proteins have been shown to interact with both positive and negative regulators of the Rho GTPase family, they may also regulate the exchange between Rab5 and Rab7 by the HOPS complex through their interaction with regulators of Rab GTPases.

It has been recently shown that the HOPS complex interacts with SAND-1/Mon1, the homologue of Mon1-Ccz1 in yeast, to promote the conversion of Rab5- into Rab7-positive endosomes (Poteryaev et al., 2010). This complex has a dual role displacing the exchange factor for Rab5, RABX-5, from early endosomes, thus interrupting the positive loop of Rab5 activation and, second, recruiting Rab7 on endosomes through its interaction with the HOPS complex (Poteryaev et al., 2007, 2010). Although both SAND-1/Mon1 and ERM proteins contribute to Rab7 recruitment to early endosomes, they appear to act toward Rab5 and its effectors through different mechanisms. Whereas SAND-1/Mon1 promotes Rab5 inactivation, our results suggest that ERM proteins have the opposite effect. Indeed, overexpression of ezrin leads to a prolonged association of EEA1 with the Rab7 endosomes and to an increased number of hybrid compartments. Thus, although more Rab7 is recruited on endosomes, the dissociation of Rab5
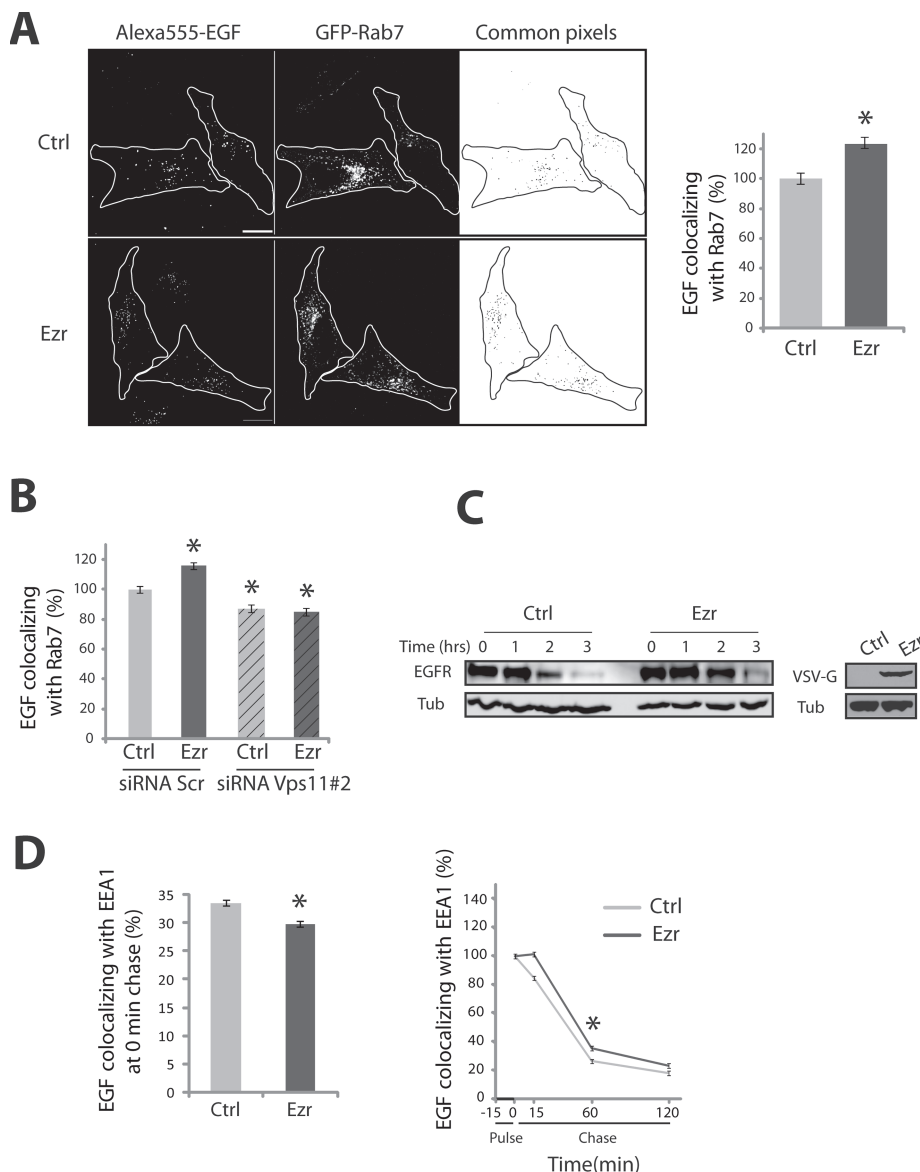
FIGURE 6: Ezrin regulates EGFR transport via the HOPS complex. (A) Colocalization of Alexa 555-EGF with GFP-Rab7 in Myc-Vps11 HeLa cells overexpressing ezrin. Right panel, the histogram represents the EGF area that overlaps with Rab7 expressed as a percentage of colocalization in control cells. Image analysis and quantification were performed as in Figure 5. Scale bar: 10 μm. (B) The histogram indicates that the increase in EGFR transport to the Rab7-positive endosomes observed in cells overexpressing ezrin requires the HOPS complex. (C) Time course of EGFR degradation in control cells and cells overexpressing ezrin (Ezr). The right panel shows the expression of exogenous ezrin. (D) Extent of EGF colocalization with EEA1 in cells overexpressing ezrin. Experiments and quantification were performed as in Figure 5. Least-square means ± SEM are plotted. Values were statistically tested using a two-way ANOVA, * $p < 0.001$.

sumably through the CORVET complex, but also the maturation of early-to-late endosomes through the HOPS complex. Knockdown of Vps11 would lead to defective EEA1 compartments that are unable to undergo homotypic fusion and maturation.

Several components of the machinery that participates in the endosomal transport including the HOPS complex are evolutionarily conserved from yeast to mammals. In contrast, ERM proteins have appeared with multicellularity, providing an additional level of regulation in response to the increased complexity of the endocytic pathway.

MATERIALS AND METHODS

Plasmids and cell lines

The following plasmids were used: pcB6 VSV-G-ezrin (Algrain *et al.*, 1993), GST-ezrin (Andreoli *et al.*, 1994), GST-radixin and -moesin, a gift from C. Roy (CRBM, Montpellier, France). The cDNA encoding human Vps11 (RZPD clone IRAKp961J22140Q2) was subcloned into pCS2-Myc vector (pCS2-Myc vector was a gift from A. Gautreau, LEBS, Gif-sur-Yvette, France). pEGFP-Rab7 was a gift from P. Chavrier (Institut Curie, Paris, France). The cDNA encoding Rab7 was subcloned into pcDNA 3.1/His/GFP vector (from A. Gautreau).

HeLa cells stably expressing myc-Vps11 were obtained by electroporation of the plasmid followed by selection in Dulbecco's modified Eagle's medium (DMEM) (Invitrogen, Carlsbad, CA) containing 10% fetal bovine serum and G418 at 0.7 g/l under 10% CO_2. Clones of HeLa cells stably coexpressing myc-Vps11 and GFP-Rab7 were selected in DMEM containing 10% fetal bovine serum, G418 at 0.6 g/l, and Hygromycin B at 0.5 g/l (InvivoGen, San Diego, CA).

Antibodies

The following primary antibodies were used: affinity-purified rabbit polyclonal anti–vesicular stomatitis virus glycoprotein tag (VSV-G) and anti-ezrin antibodies (Algrain *et al.*, 1993); monoclonal anti-ezrin antibody clone 4G11B5, a gift from Geneviève Choquet-Kastylevsky (New Markers Department, bio-Mérieux, Marcy l'Etoile, France); monoclonal anti-VSVG (clone P5D4) (Kreis, 1986), polyclonal anti-Myc antibody generated in the laboratory; anti-ERM protein antibody and anti-EGFR antibody (Cell Signaling Technology, Beverly, MA); mouse monoclonal anti-Myc (clone 9E10); mouse monoclonal anti-α tubulin (Sigma-Aldrich, St. Louis, MO); monoclonal mouse antibodies anti-Lamp1, -EEA1, -CD63 (BD Biosciences). Secondary antibodies: horseradish peroxidase- and Cy3-, Texas Red-, Cy5-conjugated goat anti–rabbit and anti–mouse (Jackson ImmunoResearch Laboratories, West Grove, PA); Alexa 488–conjugated goat anti–rabbit and anti–mouse (Molecular Probes, Eugene, OR).

and its effectors is prevented when ezrin is overexpressed, therefore impairing the maturation of endosomes. Thus, the balance between ERM proteins and SAND-1/Mon1 might establish the cut-out switch predicted in the kinetic model of Rab conversion (Del Conte-Zerial *et al.*, 2008). Because ERM proteins and SAND-1/Mon1b bind Vps11 and they both have a positive effect on Rab7 recruitment, it will be interesting to determine whether these proteins cooperate in this process.

Upon depletion of Vps11, a reduced number of hybrid EEA1/Rab7 endosomes is observed. This finding indicates that depletion of Vps11 likely affects homotypic fusion of early endosomes pre-
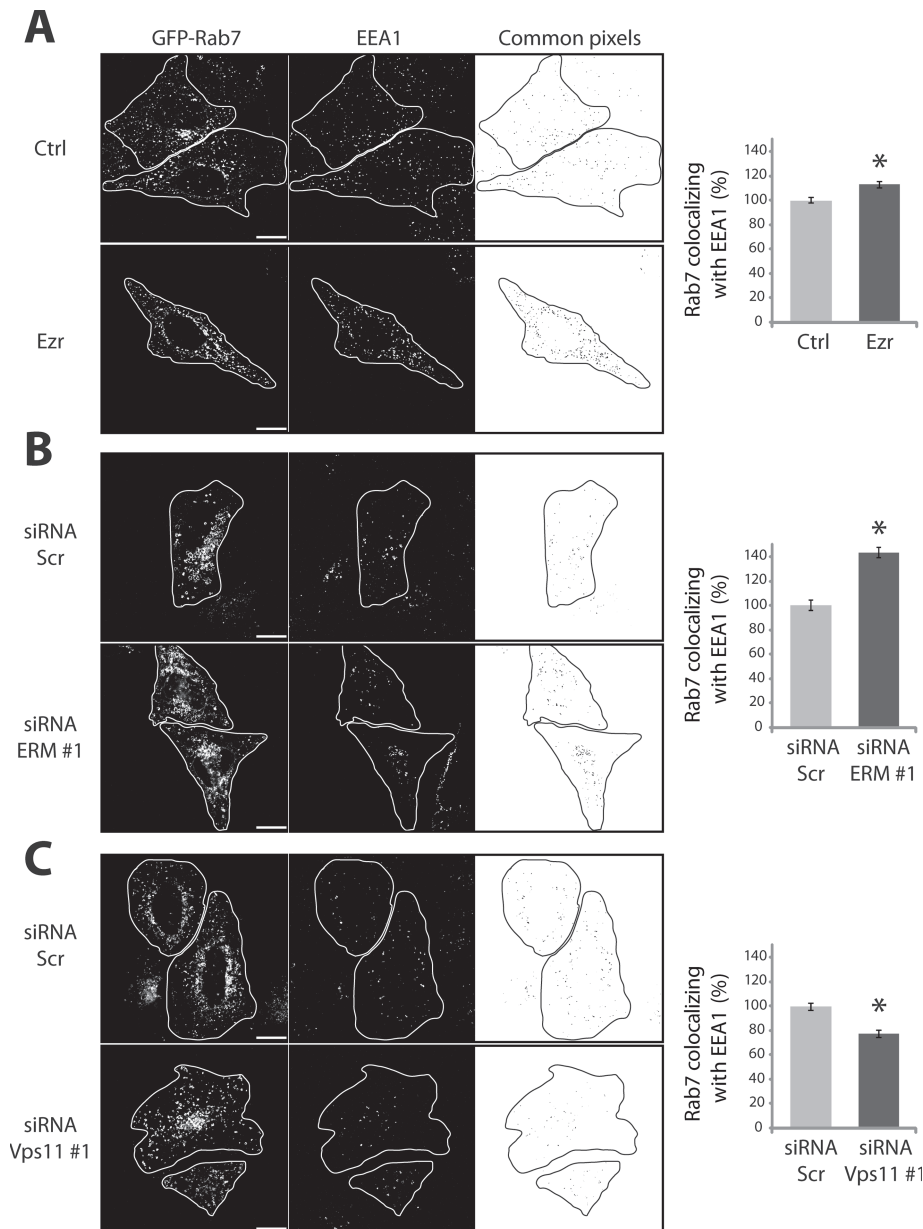
FIGURE 7: ERM proteins and the HOPS complex regulate the early-to-late endosome maturation. Colocalization of GFP-Rab7 and EEA1 in cells treated with EGF and overexpressing ezrin (A), depleted of ERM proteins (B), or depleted of Vps11 (C). Images were taken with a 3D wide-field optical sectioning microscope. The overlays represent the common pixels between respective channels after deconvolution and segmentation. Each image corresponds to a maximum-intensity Z projection. Scale bar: 10 μm. The histograms represent the Rab7 area that overlaps with EEA1 expressed as a percentage of the colocalization in control cells. Least-square means ± SEM are plotted. Statistical analysis was applied as in Figure 4.

RNA interference

For depletion of Vps11, myc-Vps11 HeLa cells were transfected with a mix of two siRNAs from On-TARGETplus siRNA (Dharmacon) using Lipofectamine RNAiMAX (Invitrogen) and then re-transfected after 48 h with the same mix. Each experiment was performed with two different sets of oligonucleotides at a concentration of 10 nM. The sequences of the siRNAs used are the following. Set #1: sense UAUUUGAGAUGGCGAUUAAUU; ACUCGAAUCUUCCCUGCUAUU. Set #2: sense GAACGUCCA-GUCCUAUAUAUU; UUUAGAGGCUACCUUAUCAUU. For depletion of ERM proteins, HeLa or myc-Vps11 HeLa cells were trans-

fected with a mix of three oligonucleotides at a concentration of 10 nM each (On-TARGETplus siRNA; Dharmacon) targeting the three proteins. Cells were analyzed 4 d after the transfection. In each experiment, two independent sets of oligonucleotides were used. Set #1: ezrin GCGCGGAGCUGUCUAGUGAUU; radixin GGCAUUAAGUUCAGAAUUA; moesin UCGCAAGCCUGAUACCAUU. Set #2: ezrin GGAAUCAACUAUUUCGAGAUU radixin CUACAUGGCUUAAACUAAA; moesin GGCUGAAACUCAAUAAGAA. ON-TARGETplus Nontargeting siRNA was used as a control.

Yeast two-hybrid screen

Yeast two-hybrid screens were performed with ezrin baits to screen at saturation a highly complex, random-primed cDNA library from human placenta using a previously described mating protocol (Formstecher et al., 2005).

Immunoprecipitation and GST pull-down experiments

For GST pull-down experiments, cells were lysed in RIPA buffer A containing 50 mM HEPES (pH 7.5), 150 mM NaCl, 10 mM EGTA, 1.5 mM MgCl$_2$, 10% glycerol, 0.1% SDS, 0.5% sodium deoxycholate, and protease inhibitor cocktail (Sigma). Clarified supernatants were incubated for 2 h at 4°C with immobilized GST fusion proteins on glutathione Sepharose 4B beads (GE Healthcare, Chalfont St. Giles, UK). For immunoprecipitation, cells were lysed in RIPA lysis buffer B (50 mM HEPES, pH 7.5, 150 mM NaCl, 10 mM EDTA, 0.1% SDS, 0.5% sodium deoxycholate, 1% Nonidet P40, and protease inhibitor cocktail). Clarified supernatants were incubated for 2 h at 4°C with antibody and protein G–Sepharose beads (Perbio, Aalst, Belgium).

EGFR degradation assay

Myc-Vps11 HeLa cells were plated at 70% of confluence, starved in serum-free DMEM for 1 h in the presence of cycloheximide (10 μg/ml; Sigma), and then incubated with DMEM supplemented with EGF (50 ng/ml; Abcam, Cambridge, MA) and cycloheximide. At the indicated time points, the cells were lysed in RIPA buffer B, and the lysates were analyzed by SDS–PAGE on 3–8% gradient NuPAGE Tris-acetate gels (Invitrogen). Western blots were analyzed by chemiluminescence with the illuminator Fuji LAS-3000 (Fujifilm, Tokyo, Japan).

EGF internalization assay

Myc-Vps11 HeLa cells grown on glass coverslips were starved in serum-free DMEM for 1 h and then treated with Alexa-555 EGF (100 ng/ml; Molecular Probes) or EGF (50 ng/ml; Abcam) for 15 min at 37°C. Cells were washed twice and chased at 37°C in serum-free
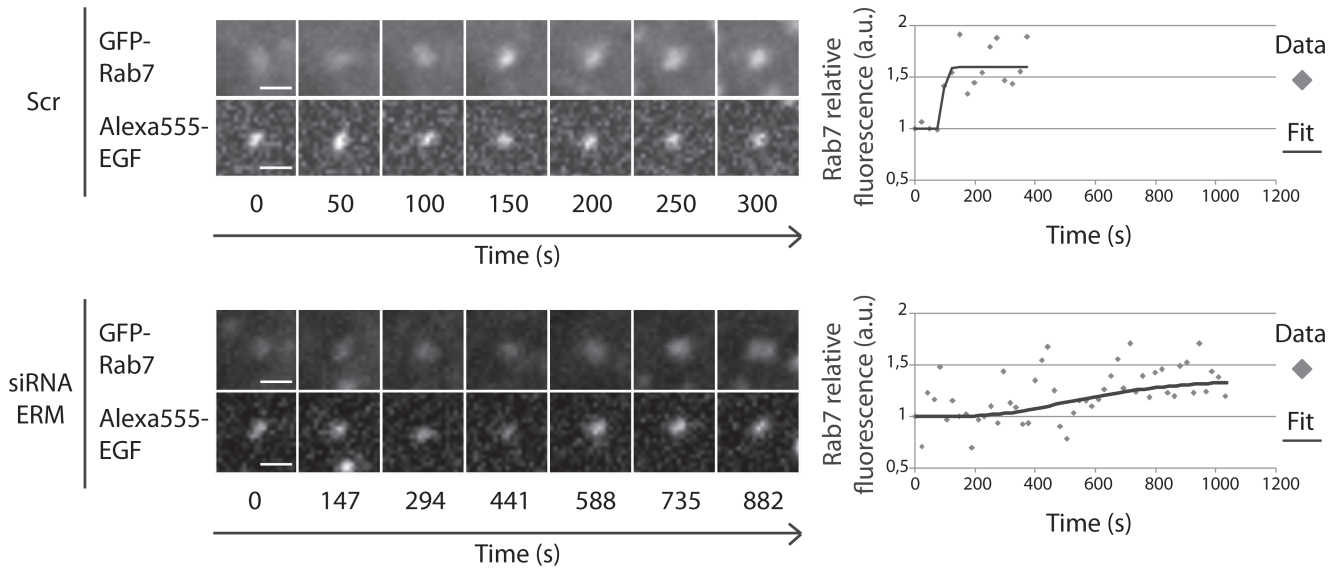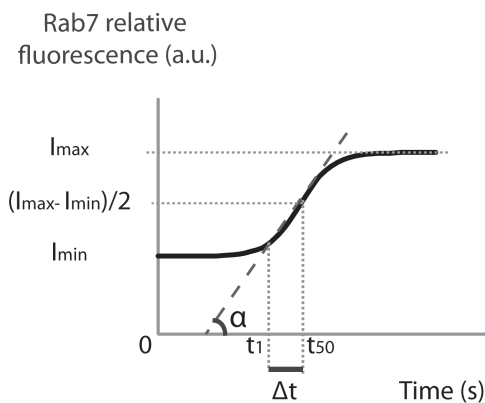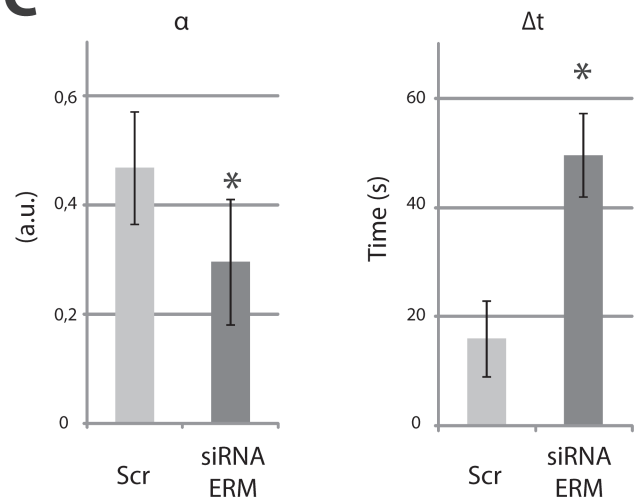
FIGURE 8: Kinetics of Rab7 recruitment on individual endosome. (A) myc-Vps11 HeLa cells stably expressing GFP-Rab7 were transfected with scramble siRNA (top panel) and siRNA targeting ERM proteins (bottom panel). Cells were imaged with a spinning disc confocal microscope during continuous uptake of Alexa555-EGF in presence of nocodazole at 37°C. The fuorescence of each fluorophore, corresponding to the projection of five planes over time, is shown for a representative endosome. Scale bar: 1 µm. Right panels, quantification of the relative fluorescence intensity of GFP-Rab7 scaled to EGF signal is represented over time for the same endosome shown in the left panel. (B) The two parameters used in subsequent analyses were calculated from the sigmoid curves obtained as described in *Materials and Methods*. (C) α and Δt were calculated from a total of 50–60 endosomes per condition and in three independent experiments. Least-square means ± SEM are plotted. Differences were statistically tested using a two-way ANOVA (* $p < 0.001$).

medium. At the indicated time points, cells were fixed with 4% paraformaldehyde and processed for immunofluorescence.

Colocalization analysis

For colocalization studies on fixed cells, we used a 90i upright Nikon Microsystems Microscope equipped with PIFOC Objective stepper and a 100X/1.4 NA Plan Apochromat objective. Slices were acquired along the Z axis every 0.2 µm to cover the entire height of the cell. Deconvolution was done by the Metamorph module (Roper Scientific, Sarasota, FL) using the Meinel algorithm. For quantification of

EGF and EEA1 colocalization, endosomes were identified on the deconvolved images using Multidimensional Image Analysis (MIA), a custom segmentation algorithm software based on wavelets (Racine et al., 2007).

Quantification of the colocalization of EGF with the different markers was performed at the single cell level. The percentage of EGF area that overlaps with EEA1 was measured for each plane using Metamorph software. Colocalization between EGF and EEA1 within each cell was calculated as the average between the values obtained for the different planes. The values reported in the graphs represent

the percentage of the colocalization between EGF and EEA1 at a 0-min chase for each condition. A minimum of 50 cells were analyzed at each time point, and differences in the colocalization of EGF and EEA1 were statistically tested using a two-way analysis of variance (ANOVA) model with interaction (SigmaStat, Systat Software Inc., Chicago, IL) on raw data before transformation into percentage. The two effects included in the ANOVA model were the treatment and the time. The data correspond to two independent experiments. The pairwise comparisons were performed with the Student-Newman-Keuls method using an α risk of 0.05. After transformation in percentage, the values were still statistically significant. The same quantification and statistical methods were applied for the analysis of the colocalization of EGF with GFP-Rab7 and GFP-Rab7 with EEA1.

Measurement of Rab7 recruitment on individual endosomes

Myc-Vps11 HeLa cells stably transfected with GFP-Rab7 were plated on glass-bottom plates (IWAKI, Lennox, Dublin, Ireland) coated with collagen type I at 6.6 µg/ml (BD Biosciences). Cells were allowed to spread for 2 h 30 min in DMEM supplemented with 10% fetal bovine serum at 37°C. Cells were then starved in serum-free L-15 in the presence of 10 µM nocodazole at 37°C for 1 h to reduce the movement of endosomes and their fusion. Alexa-555 EGF (100 ng/ml) was added, and cells were imaged at 37°C using a spinning disc confocal microscope based on a Nikon TE2000-E inverted microscope equipped with a 100X NA 1.4 oil immersion objective, a Yokogawa CSU22 spinning disk head, a NanoScanZ piezo focusing stage (Prior Scientific, Rockland, MA), a CoolSnap HQ2 camera (Photometrics, Tucson, AZ), and a temperature control chamber, The Cube (Life Imaging Services, Basel, Switzerland). X-Y multipositions were acquired using a motorized scanning stage (Marzhauser, Wetzlar, Germany). Five slices were acquired along the Z axis every 0.3 µm per time point, and the two channels were acquired sequentially at each Z position. Binning was set up to 2, and frame rate was 1 image every ~22 s for 90 min. Maximum intensity projection along the Z axis was performed, and movies were analyzed using ImageJ software (Abramoff et al., 2004). Vesicle tracking was performed manually on the EGF signal using the MtrackJ plug-in created by Eric Meijering. Only endosomes that could be tracked unambiguously were analyzed. The endosomes undergoing fusion or those too close to the adjacent ones were excluded from the analysis. Tracks were imported into the Manual Tracking plug-in (developed by Fabrice Cordelières, http://rsbweb.nih.gov/ij/plugins/track/track.html) for fluorescence quantification after background subtraction and photobleaching correction. For each endosome, the intensity of GFP-Rab7 was scaled to the EGF signal to avoid fluctuations caused by the movements in and out of the acquisition plane. Curve fitting was performed using the following logistic Hill-like equation:

$$I_{(x)} = I_{min} + \frac{(I_{max} - I_{min})}{1 + \left(\dfrac{t}{t_{50}}\right)^{h}}$$

with $t_{50} = t$ when $I = (I_{max} - I_{min})/2$. h = "Hill coefficient."

The slope α and the time Δt were determined with the following equations:

$$\alpha = \left(\frac{dI}{dt}\right)_{t=t_{50}} = \frac{-h(I_{max} - I_{min})}{4t_{50}} \text{ and } \Delta t = \frac{-2t_{50}}{h}$$

Δt and α were calculated after curve fitting for each endosome. Values obtained from three independent experiments (a total of 50–60 endosomes were analyzed per condition) were statistically tested

using a two-way ANOVA model with interaction (SigmaStat). The pairwise comparisons were performed with the Student–Newman–Keuls method using an α risk of 0.05.

Electron microscopy

HeLa myc-Vps11cells were starved in serum-free DMEM for 1 h and then pulsed with DMEM supplemented with EGF (50 ng/ml) for 15 min at 37°C. Cells were washed twice with DMEM at 4°C and then fixed for 30 min with a mixture of 2% paraformaldehyde and 0.125% glutaraldehyde in DMEM and for 2 h with 2% paraformaldehyde and 0.125% glutaraldehyde in phosphate buffer (0.1 M, pH 7.4) at room temperature. Cells were processed for ultracryomicrotomy and single immunogold labeled using protein A conjugated to 10 nm gold (PAG10) as described previously (Slot and Geuze, 2007). Sections were observed under an electron microscope (Philips CM120; FEI Company, Eindoven, The Netherlands), and images were acquired with a numeric camera (Keen View; Soft Imaging System, Münster, Germany).

REFERENCES

Abramoff MD, Magelhaes PJ, Ram SJ (2004). Image processing with ImageJ. Biophotonics Int 11, 36–42.

Algrain M, Turunen O, Vaheri A, Louvard D, Arpin M (1993). Ezrin contains cytoskeleton and membrane binding domains accounting for its proposed role as a membrane-cytoskeletal linker. J Cell Biol 120, 129–139.

Andreoli C, Martin M, Leborgne R, Reggio H, Mangeat P (1994). Ezrin has properties to self-associate at the plasma membrane. J Cell Sci 107, 2509–2521.

Barroso-Gonzalez J, Machado JD, Garcia-Exposito L, Valenzuela-Fernandez A (2009). Moesin regulates the trafficking of nascent clathrin-coated vesicles. J Biol Chem 284, 2419–2434.

Bretscher A, Edwards K, Fehon RG (2002). ERM proteins and merlin: integrators at the cell cortex. Nat Rev Mol Cell Biol. 3, 586–599.

Cha B, Tse M, Yun C, Kovbasnjuk O, Mohan S, Hubbard A, Arpin M, Donowitz M (2006). The NHE3 juxtamembrane cytoplasmic domain directly binds ezrin: dual role in NHE3 trafficking and mobility in the brush border. Mol Biol Cell 17, 2661–2673.

Defacque H et al. (2000). Involvement of ezrin/moesin in de novo actin assembly on phagosomal membranes. EMBO J 19, 199–212.

Del Conte-Zerial P, Brusch L, Rink JC, Collinet C, Kalaidzidis YM, Zerial M, Deutsch A (2008). Membrane identity and GTPase cascades regulated by toggle and cut-out switches. Mol Syst Biol 4, 206.

Fiévet BT, Gautreau A, Roy C, Del Maestro L, Mangeat P, Louvard D, Arpin M (2004). Phosphoinositide binding and phosphorylation act sequentially in the activation mechanism of ezrin. J Cell Biol 164, 653–659.

Formstecher E et al. (2005). Protein interaction mapping: a Drosophila case study. Genome Res 15, 376–384.

Gary R, Bretscher A (1995). Ezrin self-association involves binding of an N-terminal domain to a normally masked C-terminal domain that includes the F-actin binding site. Mol Biol Cell 6, 1061–1075.

Grosshans BL, Ortiz D, Novick P (2006). Rabs and their effectors: achieving specificity in membrane traffic. Proc Natl Acad Sci USA 103, 11821–11827.

Harder T, Kellner R, Parton RG, Gruenberg J (1997). Specific release of membrane-bound annexin II and cortical cytoskeletal elements by sequestration of membrane cholesterol. Mol Biol Cell 8, 533–545.

Huizing M, Didier A, Walenta J, Anikster Y, Gahl WA, Krämer H (2001). Molecular cloning and characterization of human VPS18, VPS 11, VPS16, and VPS33. Gene 264, 241–247.

Kreis TE (1986). Microinjected antibodies against the cytoplasmic domain of vesicular stomatitis virus glycoprotein block its transport to the cell surface. EMBO J 5, 931–941.

Li Q, Nance MR, Kulikauskas R, Nyberg K, Fehon R, Karplus A, Bretscher A, Tesmer JJG (2007). Self-masking in an intact ERM-merlin protein: an active role for the central a-helical domain. J Mol Biol 365, 1446–1459.

Maldonado E, Hernandez F, Lozano C, Castro ME, Navarro RE (2006). The zebrafish mutant vps18 as a model for vesicle-traffic related hypopigmentation diseases. Pigment Cell Res 19, 315–326.

Morel E, Parton RG, Gruenberg J (2009). Annexin A2-dependent polymerization of actin mediates endosome biogenesis. Dev Cell 16, 445–457.

Nickerson DP, Brett CL, Merz AJ (2009). Vps-C complexes: gatekeepers of endolysosomal traffic. Curr Opin Cell Biol 21, 543–551.

Nordmann M, Cabrera M, Perz A, Bröcker C Ostrowicz CC, Engelbrecht-Vandré S, Ungermann C (2010). The Mon1-Ccz1 complex is the GEF of the late endosomal Rab7 homolog Ypt7. Curr Biol 20, 1654–1659.

Peplowska K, Markgraf DF, Ostrowicz CW, Bange G, Ungermann C (2007). The CORVET tethering complex interacts with the yeast Rab5 homolog Vps21 and is involved in endo-lysosomal biogenesis. Dev Cell 12, 739–750.

Poteryaev D, Datta S, Ackema K, Zerial M, Spang A (2010). Identification of the switch in early-to-late endosome transition. Cell 141, 497–508.

Poteryaev D, Fares H, Bowerman B, Spang A (2007). Caenorhabditis elegans SAND-1 is essential for RAB-7 function in endosomal traffic. EMBO J 26, 301–312.

Poupon V, Stewart A, Gray SR, Piper RC, Luzio JP (2003). The role of mVps18p in clustering, fusion, and intracellular localization of late endocytic organelles. Mol Biol Cell 14, 4015–4027.

Pulipparacharuvil S, Akbar MA, Ray S, Sevrioukov EA, Haberman AS, Rohrer J, Krämer H (2005). Drosophila Vps16A is required for trafficking to lysosomes and biogenesis of pigment granules. J Cell Sci 118, 3663–3673.

Racine V, Sachse M, Salamero J, Fraisier V, Trubuil A, Sibarita JB (2007). Visualization and quantification of vesicle trafficking on a three-dimensional cytoskeleton network in living cells. J Microsc 225, 214–228.

Rieder SE, Emr SD (1997). A novel RING finger protein complex essential for a last step in protein transport to the yeast vacuole. Mol Biol Cell 8, 2307–2327.

Rink J, Ghigo E, Kalaidzidis Y, Zerial M (2005). Rab conversion as a mechanism of progression from early to late endosomes. Cell 122, 735–749.

Seals DF, Eltzen G, Margolis N, Wickner WT, Price A (2000). A Ypt/Rab effector complex containing the Sec1 homolog Vps33p is required for homotypic vacuole fusion. Proc Natl Acad Sci USA 97, 9402–9407.

Sevrioukov EA, He JP, Moghrabi N, Sunio A, Krämer H (1999). A role for the deep orange and carnation eye color genes in lysosomal delivery in Drosophila. Mol Cell 4, 479–486.

Simonsen A, Lippé R, Christoforidis S, Gaullier JM, Brech A, Callaghan J, Toh BH, Murphy C, Zerial M, Stenmark H (1998). EEA1 links PI(3)K function to Rab5 regulation of endosome fusion. Nature 394, 494–498.

Slot JW, Geuze HJ (2007). Cryosectioning and immunolabeling. Nat Protoc 2, 2480–2491.

Stanasila L, Abuin L, Diviani D, Cotecchia S (2006). Ezrin directly interacts with the alpha1b-adrenergic receptor and plays a role in receptor recycling. J Biol Chem 281, 4354–4363.

Suzuki T, Oiso N, Gautam R, Novak EK, Panthier JJ, Suprabha PG, Vida T, Swank RT, Spritz RA (2003). The mouse organellar biogenesis mutant buff results from a mutation in Vps33a, a homologue of yeast vps33 and Drosophila carnation. Proc Natl Acad Sci USA 100, 1146–1150.

Tamma G, Klussmann E, Oehlke J, Krause E, Rosenthal W, Svelto M, Valenti G (2005). Actin remodeling requires ERM function to facilitate AQP2 apical targeting. J Cell Sci 118, 3623–3630.

Turunen O, Wahlström T, Vaheri A (1994). Ezrin has a COOH-terminal actin-binding site that is conserved in the ezrin protein family. J Cell Biol 126, 1445–1453.

Vonderheit A, Helenius A (2005). Rab7 associates with early endosomes to mediate sorting and transport of Semliki forest virus to late endosomes. PloS Biol 3, e233.

Wurmser AE, Sato TK, Emr SD (2000). New component of the vacuolar class C-Vps complex couples nucleotide exchange on the Ypt7 GTPase to SNARE-dependent docking and fusion. J Cell Biol 151, 551–562.

Zhao H, Shiue H, Palkon S, Wang Y, Cullinan P, Burkhardt JK, Musch MW, Chang EB, Turner JR (2004). Ezrin regulates NHE3 translocation and activation after Na+-glucose cotransport. Proc Natl Acad Sci USA 101, 9485–9490.

Zhou R, Cao X, Watson C, Miao Y, Guo Z, Forte JG, Yao X (2003). Characterization of protein kinase A-mediated phosphorylation of ezrin in gastric parietal cell activation. J Biol Chem 278, 35651–35659.

Zhou R, Zhu L, Kodani A, Hauser P, Yao X, Forte JG (2005). Phosphorylation of ezrin on threonine 567 produces a change in secretory phenotype and repolarizes the gastric parietal cell. J Cell Sci 118, 4381–4391.